modelling

MDPI

Article

Classical Molecular Dynamics Simulations of Surface Modifications Triggered by a Femtosecond Laser Pulse

Vladimir Lipp [1,2,*] and Beata Ziaja [1,2,*]

[1] Institute of Nuclear Physics, Polish Academy of Sciences, Radzikowskiego 152, 31-342 Kraków, Poland
[2] Center for Free-Electron Laser Science CFEL, Deutsches Elektronen-Synchrotron DESY, Notkestr. 85, 22607 Hamburg, Germany
* Correspondence: vladimir.lipp@desy.de (V.L.); beata.ziaja-motyka@cfel.de (B.Z.)

Abstract: This work is devoted to classical molecular dynamics simulations of surface modifications (craters) drilled by single femtosecond laser pulses in silicon and diamond, materials relevant for numerous industrial applications. We propose a methodology paving the way towards a significant decrease in the simulation computational costs, which could also enable a precise estimation of the craters' size and shape.

Keywords: radiation damage; surface processing; femtosecond laser irradiation; molecular dynamics; similitude

check for updates

Citation: Lipp, V.; Ziaja, B. Classical Molecular Dynamics Simulations of Surface Modifications Triggered by a Femtosecond Laser Pulse. *Modelling* **2022**, *3*, 333–343. https://doi.org/10.3390/modelling3030021

Academic Editor: Antonio Brasiello

Received: 13 June 2022
Accepted: 25 July 2022
Published: 29 July 2022

Publisher's Note: MDPI stays neutral with regard to jurisdictional claims in published maps and institutional affiliations.

1. Introduction

Modern ultrashort laser pulses can deposit a large amount of energy into a very small volume of a solid material. This enables a precise local control of radiation-induced material damage, with numerous applications for femtosecond laser machining [1–3] and nanostructuring [4–6]. Moreover, advanced techniques like Femtosecond Laser Direct Writing (FLDW) enable efficient and precise material processing in industrial applications [7], with large flexibility. For such applications, guiding computer simulations, performed before experimental measurements, may allow us to avoid some of the expensive experimental 'blind' tests, in this way broadening the applicability and decreasing the overall cost of the laser processing. It would, therefore, be beneficial to have a predictive and computationally efficient simulation tool: (i) enabling to follow the material evolution up to an equilibrium state after the laser irradiation, and (ii) allowing for a flexible experimental geometry at a reasonable computational cost.

The existing computational models developed to describe the evolution of laser-irradiated solid materials are numerous. The approaches widely used due to their simplicity and efficiency are continuum models, such as Two-Temperature Model [8,9] and various hydrodynamic approaches [10–13]. They are relatively simple in their implementation, have low computational cost, and are capable of being implemented at the experimentally relevant spatial and temporal scales. However, their applicability is restricted in the regime of femtosecond timescales and μm-nm spatial scales due to the assumption of near-equilibrium conditions during the ongoing ultrafast phase transition processes (melting, spallation, ablation). Such assumption becomes even less justified under intense laser irradiation, when strong photoabsorption within the investigated material drives it into extreme transient states [14]. Non-equilibrium phase transition processes become then predominant [15]. The phase transition timescales can then be shorter than 1 ps, and the new-phase nuclei can reach a size corresponding to several interatomic distances only [16].

In contrast, atomistic modeling does not rely on the assumption of equilibrium as it always tracks particle trajectories. Recently, the *ab-initio* molecular dynamics (MD) approaches became more widespread thanks to the increasing computational power of

modern computers and the ongoing advances in their algorithmic components. By relying on the quantum-mechanical description of a many-electron system, they provide high precision and versatility [17–21]. High computational cost, however, still limits their applicability to smaller systems (typically, with up to 2000 atoms). Even if utilizing supercomputer facilities [22], the size of simulated systems is much smaller than the typical size of many systems studied experimentally. The same problem of high computational costs also affects the simulations using a simplified Tight-Binding Hamiltonian [23,24], although to a lesser degree.

The classical molecular dynamics (MD) then remains the simplest and computationally most efficient atomistic approach. It is based on the solution of Newtonian equations of motion for each particle in the system, using empirical or *ab initio* interatomic potentials [25]. In MD, an interatomic potential fully defines the material properties. Therefore, a reliable interatomic potential is crucial to achieving a quantitative description of laser-induced ultrafast processes and eventual material damage. It was already demonstrated in several cases that one could describe successfully the experimental findings in the laser-processing experiments with properly defined interatomic potentials [26,27]. However, those works usually relied on a specific geometry of the setups and took advantage of their intrinsic symmetry, in order to decrease the computational costs. If one cannot rely on such symmetries, a full 3D simulation is necessary to reproduce the experimental results. If the temporal and spatial scales considered are large, such simulation lies beyond the capacities of the existing computational tools, even if using the classical MD.

In this paper, we propose a simulation scheme based on the classical MD approach that should overcome the computational bottleneck. We will demonstrate its performance on the example of two widely used and studied semiconducting materials: silicon and diamond. The simulations are based on the free and open-source classical MD code, LAMMPS [28,29], which enables efficient and reliable atomistic simulations of various materials and of their response to laser-induced heating. In the next section, we describe in detail the proposed simulation scheme and its assumptions.

2. Simulation Scheme

In order to improve the computational efficiency of classical MD simulations, we propose to scale down the simulated volume by decreasing all its three dimensions proportionally (by the same factor), while keeping the geometry intact. This approach is based on the principle of similitude [30] which states that two systems exhibit similar behavior if they have a geometric, kinematic, and dynamic similarity. I.e., these conditions are fulfilled if the two systems are made geometrically similar, and if the ratios of all the pertinent forces are the same in the two systems. In our case, this, in particular, implies that the "scaled-down" simulation volume should still represent a sufficiently large volume in the material, and not be a conglomerate of a few atomic layers which have very different properties than bulk material.

We apply this approach to predict crater shapes in silicon and diamond created by a single femtosecond laser pulse arriving at normal incidence to the material and focused onto a micrometer spot. For simplicity, we assume that the absorbed laser energy is distributed homogeneously in the irradiated volume, which is a cylinder extending from the material surface down to some depth in the material. We will call this volume the "primary interaction volume". The cylinder diameter corresponds to the laser spot size. Its depth can be chosen arbitrarily. Note that according to Ref. [7], the FLDW allows us to ablate a specified amount of material with extensive dimensional flexibility.

In what follows, we will demonstrate that performing long-timescale simulations for the laser-heated *scaled-down primary interaction volume* can provide accurate predictions for *the primary interaction volume*—of a much larger size. The results are then obtained at a much lower computational cost than that estimated for the full-scale calculation. For this purpose, one should: (i) decrease the size of the laser spot and of the primary interaction depth by the same factor, (ii) perform a simulation to predict the size of the created crater,

i.e., its width and depth, and (iii) scale them up with the same factor, in order to obtain predictions for the original laser spot and the original primary interaction depth. We expect that this scheme could provide a way to significantly reduce computational efforts in future studies of laser-induced damage in solid materials.

For the simulations, we utilize a classical MD code, LAMMPS, using well-established interatomic potentials [31–33]. Figure 1 shows a schematic representation of the simulation setup. The laser irradiation comes along the Z axis, perpendicular to the target surface. The primary interaction volume has a cylindrical shape. The LAMMPS simulation supercell (shown with blue lines) is a square box of sufficiently large size to account for the subsequent cooling of the system due to the atomic heat diffusion. As we use periodic boundary conditions (PBC) in the (X,Y) plane, the lateral size of the simulation supercell should also be large enough to guarantee that the supercell and its images do not influence each other significantly.

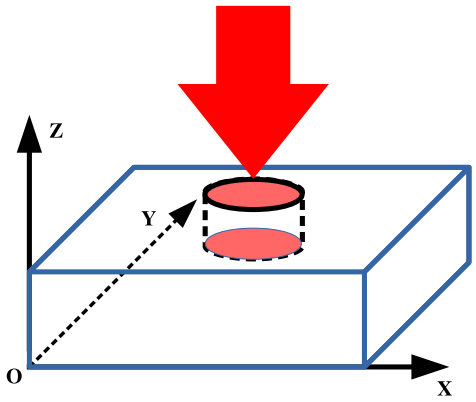

Figure 1. Schematic representation of the simulation setup.

Below we list all assumptions currently applied to simulate the evolution of the laser-heated primary interaction volume:

- *A. Primary interaction volume is a cylinder with a homogeneous distribution of absorbed energy inside.*
- *B. Classical interatomic potentials (MD) are applied.*
  As discussed above, the classical approach is optimal due to the high computational cost of other atomistic approaches and the limited applicability of the continuum methods. Here, we also do not perform explicit modeling of non-thermal effects which could induce a change in the interatomic potential due to a strong electron excitation (cf. [34]). This is justified, as, on long timescales, we expect that the nonthermal effects will lead to a similar atomic structuring as after thermal melting.
  The classical interatomic potential for silicon, which we mainly utilize in the paper [31], has been first introduced in 1985 and is still widely used to describe this material (see, e.g., [35]). It reproduces accurately not only the stable, diamond-like crystal structure of silicon but also its thermophysical properties such as equilibrium melting temperature, melting curve slope, and heat capacity [35]. Therefore, we decided to base our study on the Stillinger-Weber potential. However, in Section 3.3 we will also demonstrate that using an alternative potential [32] still supports the correctness of the similitude approach.
- *C. Thin-film supercell*
  The thin-film supercell has two free surfaces (parallel to the XY plane) and four periodic boundary surfaces (Figure 1). Such boundary conditions provide an efficient method to decrease the number of atoms in the simulation. Convergence studies performed by varying the supercell size guarantee to exclude the final-size effect.
- *D. Pressure wave cannot leave the supercell and is reflected back from the boundaries.*

In principle, one could implement dynamic non-reflective boundary conditions [36,37] in order to remove the reflected pressure waves. However, in all the cases analyzed in this work, the supercell was large enough to absorb most of the pressure waves (or the waves were weak enough to neglect them). Those observations were confirmed by the dedicated convergence studies.

- *E. Absorbed laser energy remains within the supercell.*
  We have verified that the supercell is large enough to absorb most of the heat without changing the overall atomic temperature or final crater shape in a noticeable way. If necessary for future applications, one could still add a heat sink at the boundaries, like it was done in [27], in order to fully exclude this effect.
- *F. Putting the total momentum of the crystal to zero at each time step.*
  This is necessary to avoid the drift of the computational layer supercell, caused by the momentum conservation and the escape of the ablated atoms. The ablated atoms are not affected by the change in the total momentum of the crystal.
- *G. Approximate treatment of electron-ion coupling*
  We approximate it as atomic heating with a constant rate, taking ∼0.5 ps in total. The description can be improved by using a combined MD-TTM model, similar to that published in [35]. Here, a three-dimensional treatment would be necessary. However, as we are interested in late-time predictions, the exact modeling of the heating mechanism is not necessary.
- *H. Neglecting electron transport*
  Long-timescale diffusive transport of electrons may lead to an additional electron cooling of atoms. The improvement proposed in the preceding item would also allow to include electron transport.
- *I. Actual simulation timescales (<10 ns) are shorter than those necessary to accomplish a full resolidification of the material (µs timescales).*
  Dedicated test simulations performed by us indicate that, for all the cases studied here, the resolidification should not significantly change craters' shapes. It is then not necessary to run the simulations up to µs. This simplification allows us to reduce the overall computational costs. However, an ultimate validation of this assumption would require experimental verification.

3. Results

3.1. Craters in Silicon Obtained for the Primary Interaction Depth of 590 nm

Let us first consider a silicon film irradiated by a laser beam with the spot size of 1 µm diameter in the (X,Y) plane and with the primary interaction depth of 590 nm, extending along the Z axis. As explained above, we assume that the energy absorbed from the laser is *homogeneously distributed* within a cylinder with a diameter of 1 µm and a depth of 590 nm. It is computationally not feasible to simulate the evolution of such a large material volume with an atomistic model. Therefore, we use the hypothesis of similitude: we scale the cylinder size down by 80 times in all three dimensions. The simulated interaction volume then becomes a cylinder with a diameter of 12.5 nm and a depth of 7.4 nm, containing about 46 thousand atoms. The whole MD simulation supercell has the dimensions of 54 nm by 54 nm by 27 nm along the X, Y, and Z axes, respectively, and consists of $100 \times 100 \times 50$ crystal unit cells, containing 4 million atoms in total. Such volume can be simulated on a modern supercomputer within a reasonable time. The cylinder is located centrally within the whole MD simulation supercell. For ultrashort laser pulses, the laser energy is first absorbed by the electronic subsystem in the crystal, on timescales of a few tens fs. For simplicity, we assume in our model that it happens instantaneously, i.e., at $t = 0$ ps when the lasing starts. Afterward, the electrons heat up the atoms via the electron-ion energy exchange. The corresponding atomic heating occurs in our simulation between the times, $t = 0$ ps and $t = 0.5$ ps. The latter corresponds to the timescale of the electron-ion thermalization in silicon, i.e., the temperature equilibration between the electronic and atomic subsystems.

Figure 2 shows snapshots of the section through the irradiated silicon crystal, recorded at different time instants. The absorbed dose within the primary interaction volume was 4 eV/atom. All the snapshots in this paper were generated with the help of GNU Parallel code [38]. The displayed part covers the primary interaction volume and its close surroundings in the (XZ) plane within a 3-Å thick layer extending along the Y axis. The orange rectangle corresponds to the primary interaction volume. Different coloring of the atoms indicates their different kinetic energy (given in eV). The times shown are: $t = 0$ ps (equilibrium material), $t = 50$ ps and $t = 450$ ps.

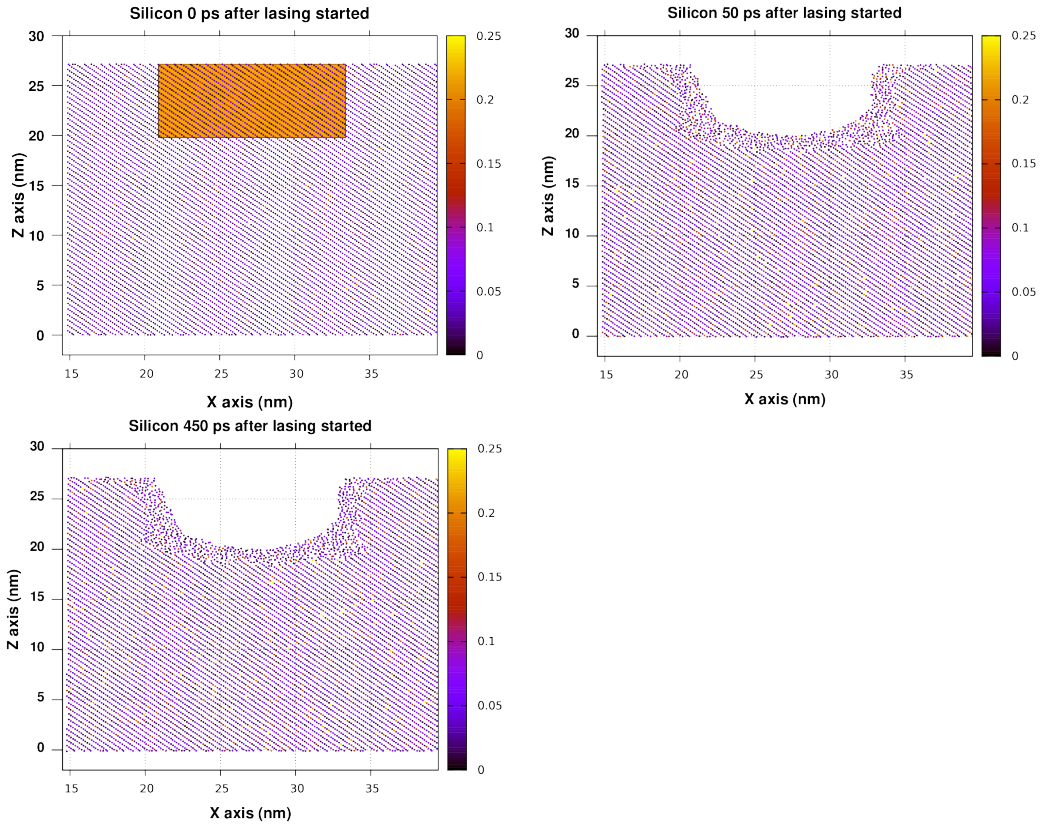

Figure 2. Snapshots showing a section through the silicon crystal after its irradiation with an ultrashort laser pulse, for the absorbed dose of 4 eV/atom within the primary interaction volume. This primary interaction volume was obtained from the original interaction volume (with a diameter of 1 μm and a depth of 590 nm), scaled down by 80 times in all three dimensions. The section includes atoms from a 0.3 nm thick layer which extends from 27.0 nm to 27.3 nm along the Y axis (including in this way the beam focus center). The supercell coordinates are: $X = (0, 54)$ nm, $Y = (0, 54)$ nm, $Z = (0, 27)$ nm. The snapshots were recorded at three different time instants. Various coloring of atoms reflects their differing kinetic energy (in eV).

As seen in Figure 2, the dose of 4 eV/atom leads to a creation of a well-shaped crater in silicon with a diameter of 13 nm (at the top) and a depth of about 7 nm (in the center). The two last snapshots show that the size of the crater does not change for at least 400 ps, indicating that the crater geometry has already become stable. Longer-timescale simulations are then not necessary.

Now, let us study the convergence of the above results with respect to the size of the primary interaction volume (i.e., the size of the cylinder), in this way testing the similitude hypothesis. Figure 3 shows the atomic snapshots for the same average absorbed dose as in Figure 2 (4 eV/atom), but with a twice larger cylinder: 25 nm in diameter, 15 nm height, consisting of about 363 thousand atoms. The cubic MD supercell is chosen to have the dimensions of 54 nm by 54 nm by 54 nm (consisting of $100 \times 100 \times 100$ crystal unit cells,

with 8 million atoms in total), in order to provide a larger environment for cooling down of the primary interaction volume (for more details, see Appendix A).

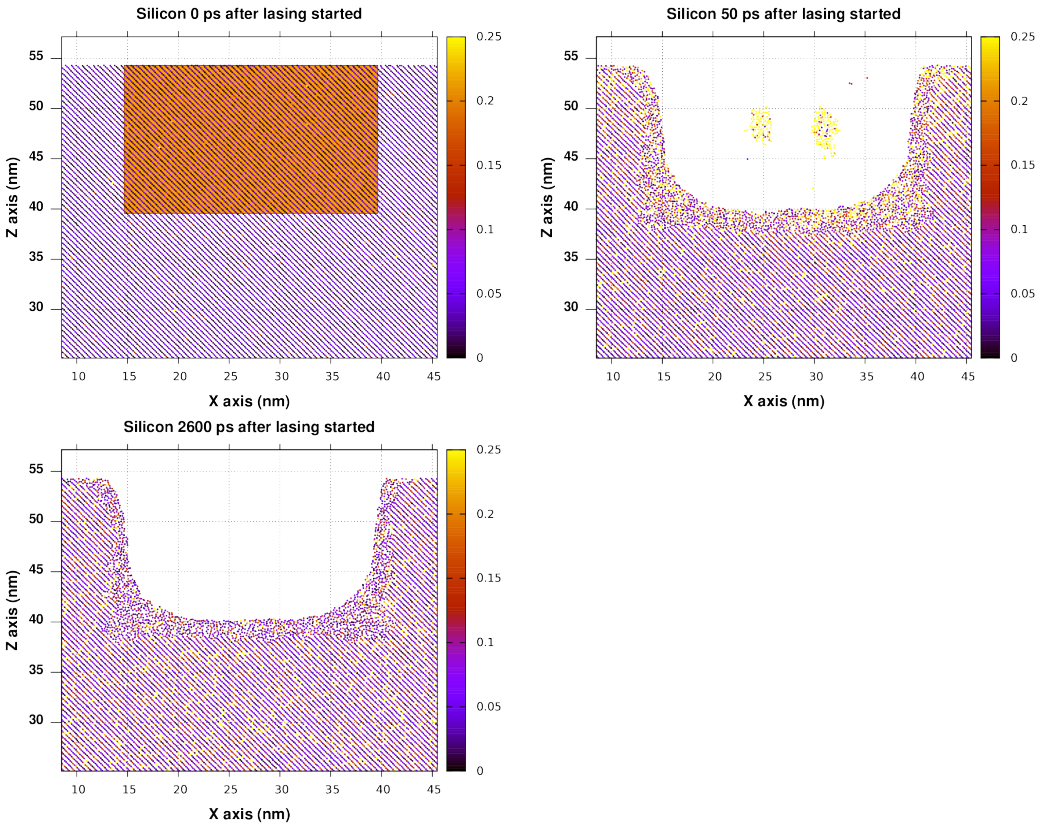

Figure 3. Snapshots showing a section through the silicon crystal after its irradiation with an ultrashort laser pulse, for the absorbed dose of 4 eV/atom within the primary interaction volume. This primary interaction volume was obtained from the original interaction volume (with a diameter of 1 μm and a depth of 590 nm), scaled down by 40 times in all three dimensions. Various coloring of atoms reflects their differing kinetic energy (in eV). The other simulation setup is the same as in Figure 2, except that the size of the whole simulation supercell was increased by a factor of 2 along the Z axis, in order to keep the overall simulation volume large enough. The supercell coordinates are: $X = (0, 54)$ nm, $Y = (0, 54)$ nm, $Z = (0, 54)$ nm. The total number of atoms in the supercell was 8 million. For convergence tests with respect to the size of the supercell, see Appendix A.

Figure 3 shows a smoothly-shaped crater with a diameter of about 27 nm (at the top) and a depth of 14 nm (in the center). These values are approximately twice larger than those obtained for the crater shown in Figure 2. This is exactly what we would expect if the hypothesis of similitude worked: for a primary interaction volume twice larger in all dimensions, we should get a crater twice larger in all dimensions, and of a similar shape.

Note that, in this case, it takes a longer time to achieve a stable crater than in the case of the smaller cylinder (Figure 2). However, the final crater shape is very similar to the final crater shape obtained for the small cylinder.

The actual result indicates that the hypothesis of similitude works for this simulation setup. To emphasize, scaling back the predicted size of the silicon craters by 80 times (Figure 2) or 40 times (Figure 3) indicates that the original laser-induced crater should have had the diameter of 1.04–1.08 μm and the depth of about 560 nm, i.e., comparable with the size of the original interaction volume. However, for full verification of the hypothesis, one would need to perform a dedicated experiment.

3.2. Craters in Silicon Obtained for the Primary Interaction Depth of 295 nm

Below we will test the similitude hypothesis for a different primary interaction depth. We perform a similar series of simulations, corresponding to the case when the laser energy has been homogeneously absorbed in a cylinder with a diameter of 1 μm and a depth of 295 nm. The corresponding simulated primary interaction volume, scaled down by 40 times, had a diameter of 25 nm, and a depth of 7.4 nm. It contains ∼182 thousand atoms. The cylinder is scaled down by 80 times and is then a cylinder with a diameter of 12.5 nm and a depth of 3.7 nm, containing ∼23 thousand atoms.

Figure 4 demonstrates that the similitude hypothesis also works for this primary interaction depth. It shows the snapshots of the section through the irradiated silicon crystal for two different laser-irradiated volumes, corresponding to the primary cylinder scaled down by 80 or by 40 times. In both cases, the craters created are well-shaped, and their sizes scale by two in all dimensions, as expected: 13 and 27 nm in width and 3 and 6.5 nm in depth, respectively.

Similarly, by scaling up the size of the silicon craters (Figure 4) by 40 or 80 times, back to the expected experimental setup size (1 μm beam spot and 295 nm depth), we predict that the original laser-induced crater should have the width of 1.04–1.08 μm and the depth of 240–260 nm. Note that the crater geometry does not change significantly after 50 ps, similarly, as for the results described above, so that we may conclude that a stable crater geometry was reached. As in the previous section, these results indicate that our suggested simulation scheme, based on the hypothesis of similitude, is applicable to the considered setup.

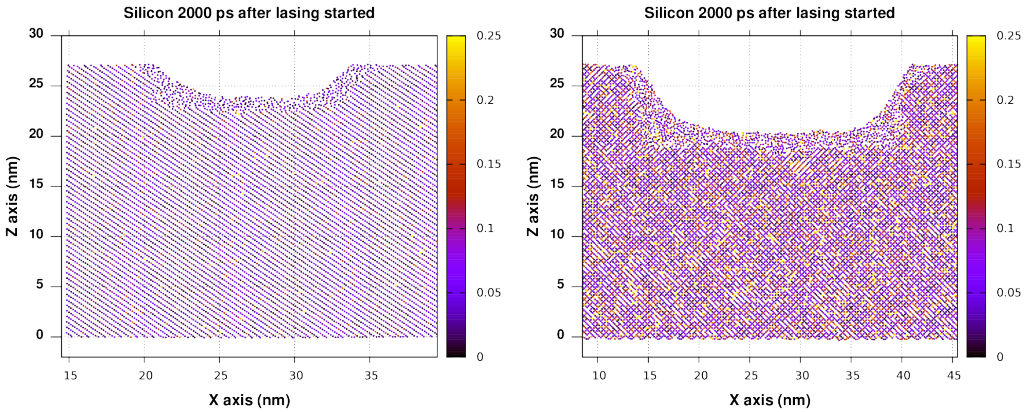

Figure 4. Snapshots showing a section through the silicon crystal after its irradiation with an ultrashort laser pulse, obtained for the absorbed dose of 4 eV/atom within the primary interaction volume. This primary interaction volume was obtained from the original interaction volume (with diameter of 1 μm and the depth of 295 nm), scaled down by 80 times (**left**) or 40 times (**right**) in all three dimensions. The other simulation setup is the same as in Figure 2, both for the left and the right snapshot.

3.3. Testing Similitude for Silicon Using the Tersoff Interaction Potential

In this section, we repeat the simulations from Section 3.1 (for the primary interaction depth of 590 nm), using Tersoff interaction potential [32]. Figure 5 shows the results for the same computational setup as in Figures 2 and 3 (compare left and right snapshots respectively). The resulting prediction for the experimental crater is noticeably different from that obtained with the Stillinger-Weber potential. This can be expected as the two potentials have very different thermophysical properties. However, the similitude principle still holds in these simulations: the size of the primary interaction volume scaled down by 80 or 40 times yields the dimensions of the craters created in silicon scaled down in the same way. The simulation set, therefore, predicts a crater of about 1.12–1.16 μm width and 640 nm depth in the center.

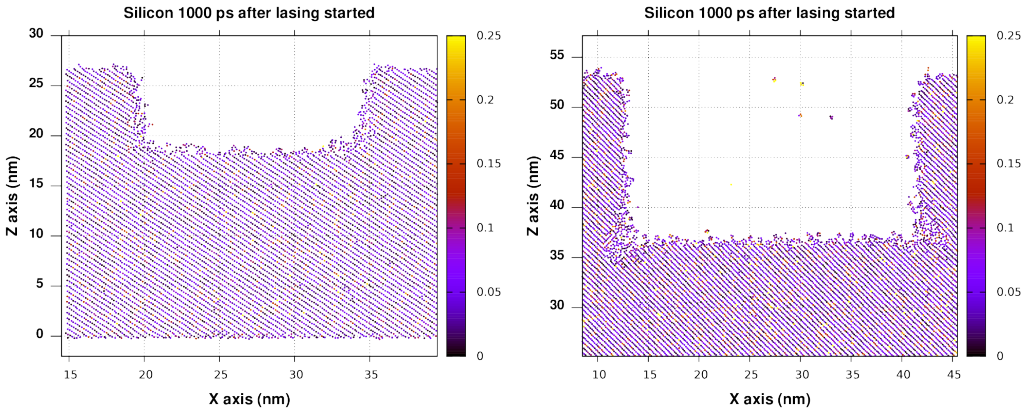

Figure 5. Snapshots showing a section through the silicon crystal after its irradiation with an ultrashort laser pulse, obtained for the absorbed dose of 4 eV/atom within the primary interaction volume. This primary interaction volume was obtained from the original interaction volume (with diameter of 1 μm and the depth of 590 nm), scaled down by 80 times (**left**) and 40 times (**right**) in all three dimensions. The supercell coordinates are: $X = (0, 54)$ nm, $Y = (0, 54)$ nm, $Z = (0, 27)$ nm (left), and $X = (0, 54)$ nm, $Y = (0, 54)$ nm, $Z = (0, 54)$ nm (right). The simulations were performed with the Tersoff potential [32].

3.4. Craters in Diamond Obtained for the Primary Interaction Depth of 181 nm

Finally, we performed the same tests for a diamond using the available LCBOP interaction potential [39]. In this case, we again assumed that the laser spot size had a 1 μm diameter, but we chose the primary interaction depth to be smaller (181 nm) than in the previous cases, in order to test how the similitude hypothesis applies for such a short depth. Figure 6 shows the snapshots obtained for the 120 times smaller primary interaction volume (left) and 80 times smaller one (right). Again, we verified that the depicted geometries did not change over 100 ps timescales. Despite single random carbon chains appearing in the small crater, which are probably not detectable, the overall shape and size of the crater obey the similitude principle quite well: scaling of both the simulated craters back to the original size yields the same result of 960 nm crater width and of about 140–170 nm depth. We conclude that the hypothesis of similitude seems reliable also in this case. However, an experimental verification would be necessary for the final validation.

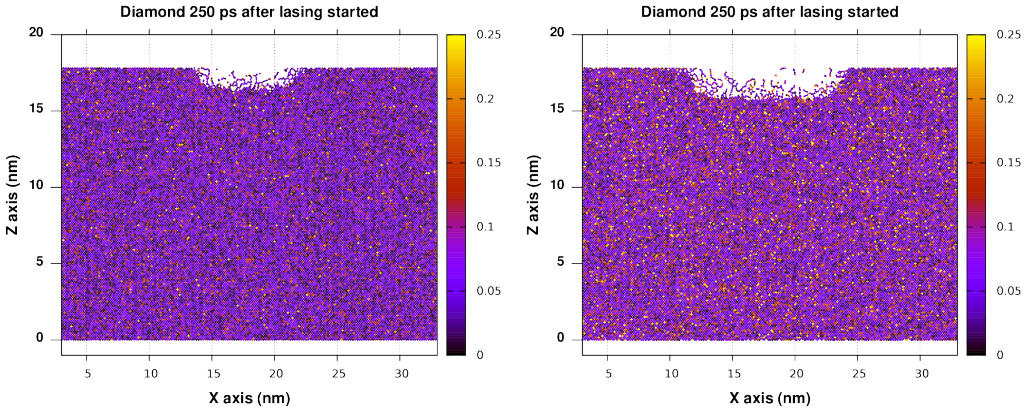

Figure 6. Snapshots showing a section through the diamond crystal irradiated with an ultrashort laser pulse, for the absorbed dose of 4 eV/atom within the primary interaction volume. This primary interaction volume was obtained from the original interaction volume (with diameter of 1 μm and the depth of 181 nm), scaled down by 120 times (**left**) and 80 times (**right**) in all three dimensions. The section includes atoms from a 3 Å thick layer which extends from 17.7 nm to 18.0 nm along the Y axis (including in this way the beam focus center). The supercell coordinates are: $X = (0, 36)$ nm, $Y = (0, 36)$ nm, $Z = (0, 18)$ nm. The results were obtained, using LCBOP potential [39].

4. Conclusions and Outlook

In order to improve the computational efficiency of classical MD simulations on laser-drilled craters in silicon and diamond, we proposed to scale down the size of the simulated volume, applying the principle of similitude. The results of our simulations indicate that this methodology can indeed significantly decrease computational costs for the considered computational setups, at the same time providing scalable predictions for the created crater's dimensions. We checked that after downscaling the primary interaction volume by 60 times for silicon and 100 times for diamond (not shown), we also obtained proportionally scaled craters, in accordance with the similitude hypothesis. Still, dedicated computational studies are required to test the applicability of the hypothesis for more complex systems than the homogeneous materials considered here. In addition, experimental validation is required to ultimately confirm the applicability of the similitude principle for the description of laser-created craters. We hope that this work will inspire dedicated experimental efforts.

In summary, we believe that this study paves the way to more efficient computer simulations of craters created in silicon and diamond by an ultrashort laser pulse. If successful, our computational approach could be utilized in the future to guide material processing with ultrafast laser pulses, minimizing or, in certain cases, even eliminating the need for expensive experimental testing.

Author Contributions: Conceptualization, B.Z.; Data curation, V.L.; Formal analysis, V.L. and B.Z.; Funding acquisition, B.Z.; Investigation, V.L.; Methodology, V.L. and B.Z.; Project administration, B.Z.; Resources, B.Z.; Software, V.L.; Supervision, B.Z.; Validation, V.L.; Visualization, V.L.; Writing—original draft, V.L.; Writing—review and editing, V.L. and B.Z. All authors have read and agreed to the published version of the manuscript.

Funding: This research was funded by the DESY Generator Program.

Data Availability Statement: The data presented in this study are available on request from the corresponding author.

Acknowledgments: We thank the DESY ITT Department members, Stephanie Maier and Ilka Mahns for helpful discussions. The simulations were performed on the DESY Maxwell cluster.

Conflicts of Interest: The authors declare no conflict of interest.

Appendix A. Convergence of Results with Respect to the Supercell Size

In this Appendix, we investigate the convergence of our results with respect to the size of the whole supercell. The proper size of the crystal surrounding the primary interaction volume is crucial to correctly simulate the heat propagation from it to the other parts of the target, as it occurs under realistic (experimental) conditions. However, in our simulations, we use periodic boundary conditions, and whenever the surrounding crystal in our simulations is too small, the heat cannot properly escape from the primary interaction volume. This can negatively affect the reliability of the model predictions. In order to identify a reasonably large size of the MD supercell, yet with relatively low computational cost resulting, we performed a size convergence study by simulating a fixed primary interaction volume (a cylinder) with two surrounding MD supercells of different sizes.

We kept the size of the primary interaction volume the same as in Figure 3, i.e., 40 times smaller than that corresponding to 590 nm primary interaction depth, but varied the number of the surrounding atoms. We performed two simulations, one with the original supercell size of 54 nm by 54 nm by 27 nm along the X, Y, and Z axis, respectively, consisting of 4 million atoms (Figure A1), and the other one with the twice larger cubic supercell: 54 nm by 54 nm by 54 nm, consisting of 8 million atoms (Figure 3, shown earlier in the paper). In the latter case, we elongated the supercell in the Z direction twice so that the laser-induced heat had more space to propagate away from the crater. When comparing these two cases, one can see that whenever the heat could not escape from the crater and its vicinity, it unphysically delayed the crater stabilization, affecting the predicted crater shape and its size (Figure A1). In the 8-million-atom supercell case, the heat accumulation

was significantly smaller. Therefore, we conclude that the supercell with 8 million atoms is sufficiently large to obtain reliable simulation predictions. For this reason, an 8 million-atom supercell was used in Sections 3.1 and 3.3 for the absorbed dose of 4 eV/atom.

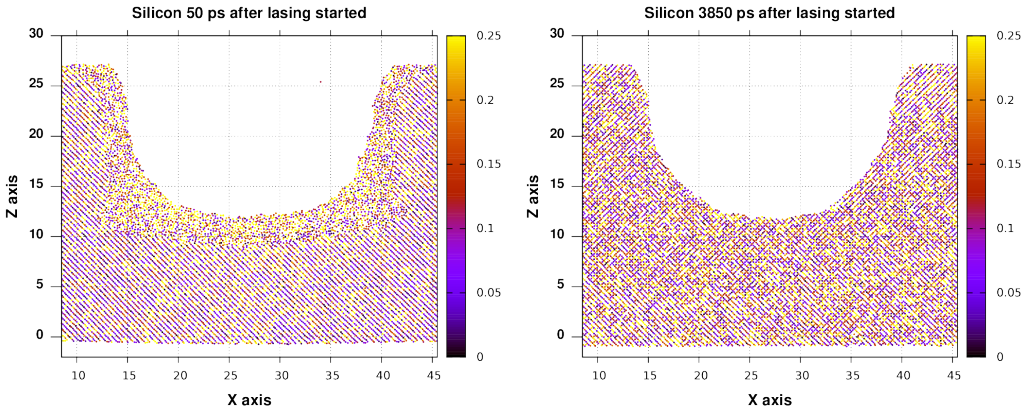

Figure A1. Snapshots showing a section through the silicon crystal after its irradiation with an ultrashort laser pulse, for the absorbed dose of 4 eV/atom within the primary interaction volume. The simulation setup is the same as in Figure 3, except the changed size of the MD simulation supercell to $X = (0, 54)$ nm, $Y = (0, 54)$ nm, $Z = (0, 27)$ nm.

We also performed an analogous convergence study for the lateral size (XY directions) of the MD supercell (not shown here). From the two studies, we generally concluded that a reliable simulation setup requires that the total absorbed dose averaged over the whole supercell should not exceed ∼0.25 eV/atom. This threshold was exceeded in Figure A1, resulting in an unreliable shape of the damage crater.

The two above-mentioned convergence studies also indicate that the reflected laser-caused pressure waves did not affect the simulation results for the chosen setup, since otherwise, we would see some differences in the crater size for different MD supercell sizes—which was not the case.

References

1. Chichkov, B.N.; Momma, C.; Nolte, S.; Von Alvensleben, F.; Tünnermann, A. Femtosecond, picosecond and nanosecond laser ablation of solids. *Appl. Phys. A* **1996**, *63*, 109–115. [CrossRef]
2. Liu, X.; Du, D.; Mourou, G. Laser ablation and micromachining with ultrashort laser pulses. *IEEE J. Quantum. Electron.* **1997**, *33*, 1706–1716. [CrossRef]
3. Gattass, R.R.; Mazur, E. Femtosecond laser micromachining in transparent materials. *Nat. Photonics* **2008**, *2*, 219–225. [CrossRef]
4. Chou, S.Y.; Keimel, C.; Gu, J. Ultrafast and direct imprint of nanostructures in silicon. *Nature* **2002**, *417*, 835–837. [CrossRef]
5. Le Harzic, R.; Schuck, H.; Sauer, D.; Anhut, T.; Riemann, I.; König, K. Sub-100 nm nanostructuring of silicon by ultrashort laser pulses. *Opt. Express* **2005**, *13*, 6651–6656. [CrossRef] [PubMed]
6. Le Harzic, R.; Dörr, D.; Sauer, D.; Stracke, F.; Zimmermann, H. Generation of high spatial frequency ripples on silicon under ultrashort laser pulses irradiation. *Appl. Phys. Lett.* **2011**, *98*, 211905. [CrossRef]
7. Terakawa, M. Femtosecond Laser Direct Writing. In *Micro and Nano Fabrication Technology*; Springer: Singapore, 2018; pp. 481–498. [CrossRef]
8. Anisimov, S.I.; Kapeliovich, B.L.; Perel'Man, T.L. Electron emission from metal surfaces exposed to ultrashort laser pulses. *Zh. Eksp. Teor. Fiz* **1974**, *66*, 375–377.
9. Van Driel, H.M. Kinetics of high-density plasmas generated in Si by 1.06-and 0.53-mkm picosecond laser pulses. *Phys. Rev. B* **1987**, *35*, 8166. [CrossRef]
10. Anisimov, S.I.; Inogamov, N.A.; Oparin, A.M.; Rethfeld, B.; Yabe, T.; Ogawa, M.; Fortov, V.E. Pulsed laser evaporation: Equation-of-state effects. *Appl. Phys. A* **1999**, *69*, 617–620. [CrossRef]
11. Grasser, T.; Tang, T.W.; Kosina, H.; Selberherr, S. A review of hydrodynamic and energy-transport models for semiconductor device simulation. *Proc. IEEE* **2003**, *91*, 251–274. [CrossRef]
12. Mazhukin, V.I.; Nikiforova, N.M.; Samokhin, A.A. Photoacoustic effect upon material melting and evaporation by laser pulses. *Phys. Wave Phenom.* **2007**, *15*, 81–94. [CrossRef]
13. Tsibidis, G.D.; Barberoglou, M.; Loukakos, P.A.; Stratakis, E.; Fotakis, C. Dynamics of ripple formation on silicon surfaces by ultrashort laser pulses in subablation conditions. *Phys. Rev. B* **2012**, *86*, 115316. [CrossRef]

14. Rethfeld, B.; Kaiser, A.; Vicanek, M.; Simon, G. Ultrafast dynamics of nonequilibrium electrons in metals under femtosecond laser irradiation. *Phys. Rev. B* **2002**, *65*, 214303. [CrossRef]
15. Remington, B.A.; Bazan, G.; Belak, J.; Bringa, E.; Colvin, J.D.; Edwards, M.J.; Glendinning, S.G.; Kalantar, D.H.; Kumar, M.; Lasinski, B.F.; et al. Materials science under extreme conditions of pressure and strain rate. *Metall. Mater. Trans. A Phys. Metall. Mater. Sci.* **2004**, *35*, 2587–2607. [CrossRef]
16. Rethfeld, B.; Sokolowski-Tinten, K.; Von der Linde, D.; Anisimov, S. Ultrafast thermal melting of laser-excited solids by homogeneous nucleation. *Phys. Rev. B* **2002**, *65*, 092103. [CrossRef]
17. Silvestrelli, P.L.; Alavi, A.; Parrinello, M.; Frenkel, D. Ab initio molecular dynamics simulation of laser melting of silicon. *Phys. Rev. Lett.* **1996**, *77*, 3149. [CrossRef]
18. Stampfli, P.; Bennemann, K.H. Theory for the instability of the diamond structure of Si, Ge, and C induced by a dense electron-hole plasma. *Phys. Rev. B* **1990**, *42*, 7163. [CrossRef]
19. Jeschke, H.O.; Garcia, M.; Lenzner, M.; Bonse, J.; Krüger, J.; Kautek, W. Laser ablation thresholds of silicon for different pulse durations: Theory and experiment. *Appl. Surf. Sci.* **2002**, *197*, 839–844. [CrossRef]
20. Zijlstra, E.S.; Kalitsov, A.; Zier, T.; Garcia, M.E. Fractional diffusion in silicon. *Adv. Mater.* **2013**, *25*, 5605–5608. [CrossRef]
21. Hao, Y.; Inhester, L.; Hanasaki, K.; Son, S.K.; Santra, R. Efficient electronic structure calculation for molecular ionization dynamics at high x-ray intensity. *Struct. Dyn.* **2015**, *2*, 041707. [CrossRef]
22. Bolnykh, V.; Olsen, J.M.H.; Meloni, S.; Bircher, M.P.; Ippoliti, E.; Carloni, P.; Rothlisberger, U. Extreme Scalability of DFT-Based QM/MM MD Simulations Using MiMiC. *J. Chem. Theory Comput.* **2019**, *15*, 5601–5613. [CrossRef]
23. Medvedev, N.; Tkachenko, V.; Lipp, V.; Li, Z.; Ziaja, B. Various damage mechanisms in carbon and silicon materials under femtosecond X-ray irradiation. *4open* **2018**, *1*, 3. [CrossRef]
24. Hourahine, B.; Aradi, B.; Blum, V.; Bonafé, F.; Buccheri, A.; Camacho, C.; Cevallos, C.; Deshaye, M.Y.; Dumitricã, T.; Dominguez, A.; et al. DFTB+, a software package for efficient approximate density functional theory based atomistic simulations. *J. Chem. Phys.* **2020**, *152*, 124101. [CrossRef]
25. Allen, M.P.; Tildesley, D.J. *Computer Simulation of Liquids*; Oxford University Press: Oxford, UK, 1989.
26. Ivanov, D.S.; Kuznetsov, A.I.; Lipp, V.P.; Rethfeld, B.; Chichkov, B.N.; Garcia, M.E.; Schulz, W. Short laser pulse nanostructuring of metals: Direct comparison of molecular dynamics modeling and experiment. *Appl. Phys. A* **2013**, *111*, 675–687. [CrossRef]
27. Ivanov, D.S.; Lipp, V.P.; Blumenstein, A.; Kleinwort, F.; Veiko, V.P.; Yakovlev, E.; Roddatis, V.; Garcia, M.E.; Rethfeld, B.; Ihlemann, J.; et al. Experimental and Theoretical Investigation of Periodic Nanostructuring of Au with Ultrashort UV Laser Pulses near the Damage Threshold. *Phys. Rev. Appl.* **2015**, *4*, 064006. [CrossRef]
28. Plimpton, S. Fast Parallel Algorithms for Short-Range Molecular Dynamics. *J. Comput. Phys.* **1995**, *117*, 1–19. [CrossRef]
29. Thompson, A.P.; Aktulga, H.M.; Berger, R.; Bolintineanu, D.S.; Brown, W.M.; Crozier, P.S.; in't Veld, P.J.; Kohlmeyer, A.; Moore, S.G.; Nguyen, T.D.; et al. LAMMPS—A flexible simulation tool for particle-based materials modeling at the atomic, meso, and continuum scales. *Comp. Phys. Comm.* **2022**, *271*, 108171. [CrossRef]
30. Kline, S.J. *Similitude and Approximation Theory*; Springer Science & Business Media: Berlin/Heidelberg, Germany, 2012.
31. Stillinger, F.H.; Weber, T.A. Computer simulation of local order in condensed phases of silicon. *Phys. Rev. B* **1985**, *31*, 5262. [CrossRef]
32. Tersoff, J. Empirical interatomic potential for silicon with improved elastic properties. *Phys. Rev. B* **1988**, *38*, 9902. [CrossRef]
33. Xie, H.; Yin, F.; Yu, T.; Wang, J.T.; Liang, C. Mechanism for direct graphite-to-diamond phase transition. *Sci. Rep.* **2014**, *4*, 5930. [CrossRef]
34. Bauerhenne, B.; Lipp, V.P.; Zier, T.; Zijlstra, E.S.; Garcia, M.E. Self-Learning Method for Construction of Analytical Interatomic Potentials to Describe Laser-Excited Materials. *Phys. Rev. Lett.* **2020**, *124*, 085501. [CrossRef]
35. Lipp, V.P.; Rethfeld, B.; Garcia, M.E.; Ivanov, D.S. Atomistic-continuum modeling of short laser pulse melting of Si targets. *Phys. Rev. B* **2014**, *90*, 245306. [CrossRef]
36. Zhigilei, V.; Garrison, B.J. Pressure Waves in Microscopic Simulations of Laser Ablation. *MRS Online Proc. Libr.* **1998**, *538*, 491–496. [CrossRef]
37. Schäfer, C.; Urbassek, H.M.; Zhigilei, L.V.; Garrison, B.J. Pressure-transmitting boundary conditions for molecular-dynamics simulations. *Comp. Mat. Sci.* **2002**, *24*, 421–429. [CrossRef]
38. Tange, O. GNU Parallel—The Command-Line Power Tool. *Login Usenix Mag.* **2011**, *36*, 42–47. [CrossRef]
39. Los, J.; Fasolino, A. Intrinsic long-range bond-order potential for carbon: Performance in Monte Carlo simulations of graphitization. *Phys. Rev. B* **2003**, *68*, 024107. [CrossRef]